Patterned Growth of Graphene over Epitaxial Catalyst

Hiroki Ago, Izumi Tanaka, Carlo M. Orofeo, Masaharu Tsuji, and Ken-ichi Ikeda*

***R**ectangle- and triangle-shaped microscale graphene films are grown on epitaxial Co films deposited on single-crystal MgO substrates with (001) and (111) planes, respectively. A thin film of Co or Ni metal is epitaxially deposited on a MgO substrate by sputtering while heating the substrate. Thermal decomposition of polystyrene over this epitaxial metal film in vacuum gives rectangular or triangular pit structures whose orientation and shape are strongly dependent on the crystallographic orientation of the MgO substrate. Raman mapping measurements indicate preferential formation of few-layer graphene films inside these pits. The rectangular graphene films are transferred onto a SiO_2/Si substrate while maintaining the original shape and field-effect transistors are fabricated using the transferred films. These findings on the formation of rectangular/triangular graphene give new insights on the formation mechanism of graphene and can be applied for more advanced/controlled graphene growth.*

Keywords:
- catalysis
- epitaxy
- graphene
- pattern formation

1. Introduction

Graphene has been attracting great interest because of its ideal two-dimensional (2D) π-conjugated network with atomic-scale thickness.[1] Single- and few-layer graphene films show excellent and unique physical properties, such as extraordinarily high carrier mobility and the quantum Hall effect.[2–7] The mechanical flexibility and high optical transparency of graphene films are useful for flexible electronics[8–10] and their high surface area can be applied to sensors.[11,12]

Mechanical exfoliation of highly-oriented pyrolytic graphite (HOPG) has been frequently used to prepare graphene films but there are broad distributions in their sizes, structures, and film thicknesses.[1] Epitaxial growth over a single-crystal SiC substrate through thermal evaporation of Si atoms also gives high-quality graphene.[13–17] Single crystals of transition metals, such as Ni(111),[18,19] Ru(0001),[20–22] and Ir(0001),[23] give well defined graphene films via catalytic pyrolysis of hydrocarbon molecules in ultrahigh vacuum. However, the single crystals of SiC and metals are very expensive and their size is limited. Thus, they are not suitable for practical applications.

Recently, chemical vapor deposition (CVD) of hydrocarbon feedstock over transition metal films has emerged as a promising method to synthesize large-area graphene films with relatively low cost.[24–28] The metal films act as a catalyst of graphene growth that generally involves decomposition of carbon feedstock, dissolution of carbon atoms into the metal film, and precipitation of graphitic carbons on the metal surface. One main problem is that these metal films are polycrystalline; either free-standing metal foils[24,28] or evaporated films deposited on Si wafers with an amorphous oxide layer (SiO_2/Si)[25–27] have been studied so far. Reflecting the polycrystalline nature of the metal catalysts, the domain size of graphene is relatively small and many domain boundaries are present in the film. Therefore, it is important to investigate a crystalline metal film as catalyst for well defined graphene synthesis. One possible approach is to use an epitaxial metal film deposited on a single-crystalline substrate, such as sapphire (α-Al_2O_3) and single-crystal MgO.[29–31] These crystalline substrates are widely used and less expensive and larger wafers

[*] Prof. H. Ago, I. Tanaka, M. Tsuji
Institute for Materials Chemistry and Engineering
Kyushu University
Kasuga, Fukuoka 816-8580 (Japan)
E-mail: ago@cm.kyushu-u.ac.jp
C. M. Orofeo, K. Ikeda
Graduate School of Engineering Sciences
Kyushu University
Kasuga, Fukuoka 816-8580 (Japan)

Supporting Information is available on the WWW under http://www.small-journal.com or from the author.

DOI: 10.1002/smll.200902405

NANO MICRO small

are commercially available compared with the single-crystal metal substrates. No studies on the catalytic growth of graphene over such epitaxial metal films have been reported to the best of our knowledge. As for the carbon source, since most of the current CVD growth utilizes methane gas,[24–28] other carbon sources are also interesting to study. Because the thickness of graphene films grown by CVD is usually controlled by the cooling rate of the substrate after reaction with methane, [24] a more simple method is expected.

In this Full Paper, we report the catalytic growth of graphene films on the epitaxial Co and Ni films deposited on single-crystal MgO substrates with (001) and (111) planes. A thin film of polystyrene (PS) was used as carbon source instead of a hydrocarbon gas and simple annealing of the PS/Co/MgO sample in vacuum resulted in graphene formation. Rectangular and triangular pit structures were formed on the Co films on MgO (001) and MgO (111) substrates respectively and graphene films were found to grow preferentially inside these pits. In addition, the rectangular graphene films were transferred onto a SiO_2/Si substrate with nearly 100% yield using a poly(methyl methacrylate) (PMMA) film. A field-effect transistor (FET) was demonstrated using the transferred graphene.

2. Results and Discussion

2.1. Characterization of Metal Catalysts

Figure 1 illustrates the experimental procedure. An epitaxial Co film of 50-nm thickness was deposited onto a single-crystal MgO substrate by radio frequency (RF) magnetron sputtering while controlling the substrate temperature. Two different substrate temperatures, room temperature (RT) and 300 °C, were studied. This substrate temperature was found to be important for the epitaxial growth, as will be discussed later. PS ($M_w = 280\,000$) was spin-coated from a tetrahydrofuran (THF) solution with 300–1000-nm thickness. Next, the PS/Co/MgO substrate was annealed in vacuum ($\approx 10^{-4}$ Pa) at 900 °C for 10–30 min.

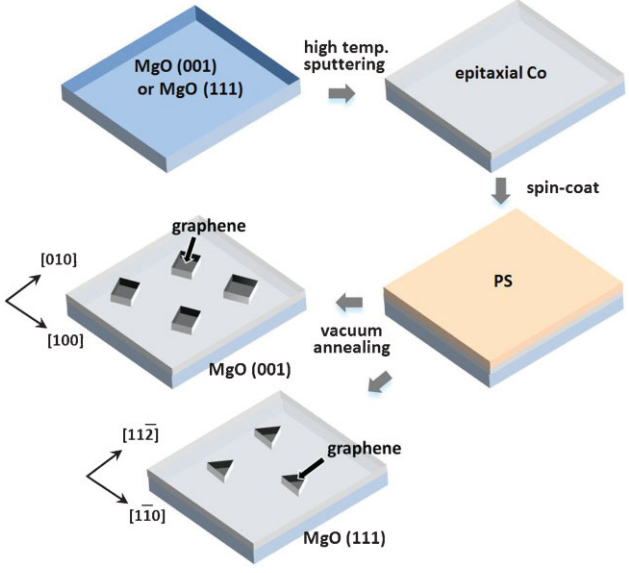

Figure 1. Preparation process of rectangular and triangular graphene over epitaxial Co films deposited on MgO (001) and MgO (111) substrates, respectively.

First, we studied the quality of the Co films deposited on MgO(100) substrates by using X-ray diffraction (XRD). When Co was deposited on the MgO substrate without heating, no diffraction peak was observed from the Co film (Figure 2a, lower), suggesting an amorphous structure. On the other hand, when sputtered at high substrate temperature, the deposited Co showed a clear diffraction peak from a β-Co(002) plane (Figure 2b, lower). The β-Co phase corresponds to a face-centered cubic (fcc) structure. This result indicates the formation of a crystalline Co film with the surface parallel to MgO(001) plane, denoted β-Co(001)//MgO(001). We annealed these Co/MgO substrates at 900 °C for 30 min in vacuo to observe the change in the crystallinity of the Co films (Figure 2a and b, upper). The crystallinity was greatly improved for both samples. However, as shown in the inset of Figure 2a, the RT-sputtered film coalesced significantly and lost the continuous film structure after vacuum annealing. In the case of the high-temperature-sputtered film, the film maintained the smooth surface even after annealing and showed the strongest Co(002) diffraction peak. Therefore, sputtering at high substrate temperature is very important for graphene synthesis because of the thermal stability and high crystallinity of Co films. It is noted that our Co thickness (50 nm) is much thinner than those used in previous CVD studies (300 nm,[27] 500 nm,[25] or thick foil[24,28]). This is advantageous because we can reduce the amount of metal catalyst and a thinner film is easier to remove for transfer processes.

Figure 2c shows an optical microscopy image of the heat-treated epitaxial Co film that was sputtered at 300 °C. A number of rectangular pits with 5–20-μm size appeared on the Co surface upon annealing. The atomic force microscopy (AFM) images of a rectangular pit are shown in the Supporting Information (Figure S1). In some of the rectangular pits, a step–terrace structure was observed at the bottom suggesting remnants of Co film, although some seem to have no Co metal at the bottom of the pit. Electron back-scattered diffraction (EBSD) was also performed for the annealed sample (Figure 2d). It was confirmed that the substrate surface is fully covered with β-Co(001) plane except for the pits. Because the EBSD was measured by inclining the sample at ≈70°, the electron beam did not fully enter into the pits so they appeared black. We found that the in-plane orientation of the Co film matches that of the underneath MgO, which can be denoted as β-Co[100]// MgO[100]. This result indicates the formation of the epitaxial Co film on the MgO(100) substrate. It is likely that observed rectangular pits originated in the lattice strain inside the Co film because of the large mismatch between the lattice constants of β-Co (0.354 nm) and MgO (0.421 nm). During substrate heating, pits are created on the Co surface to release this lattice strain. Considering the orientation of the pits and the slope of their sidewall, we speculate that the Co(111) surface that appeared at the sidewall of the pits is due to the relative stability of the (111) plane.

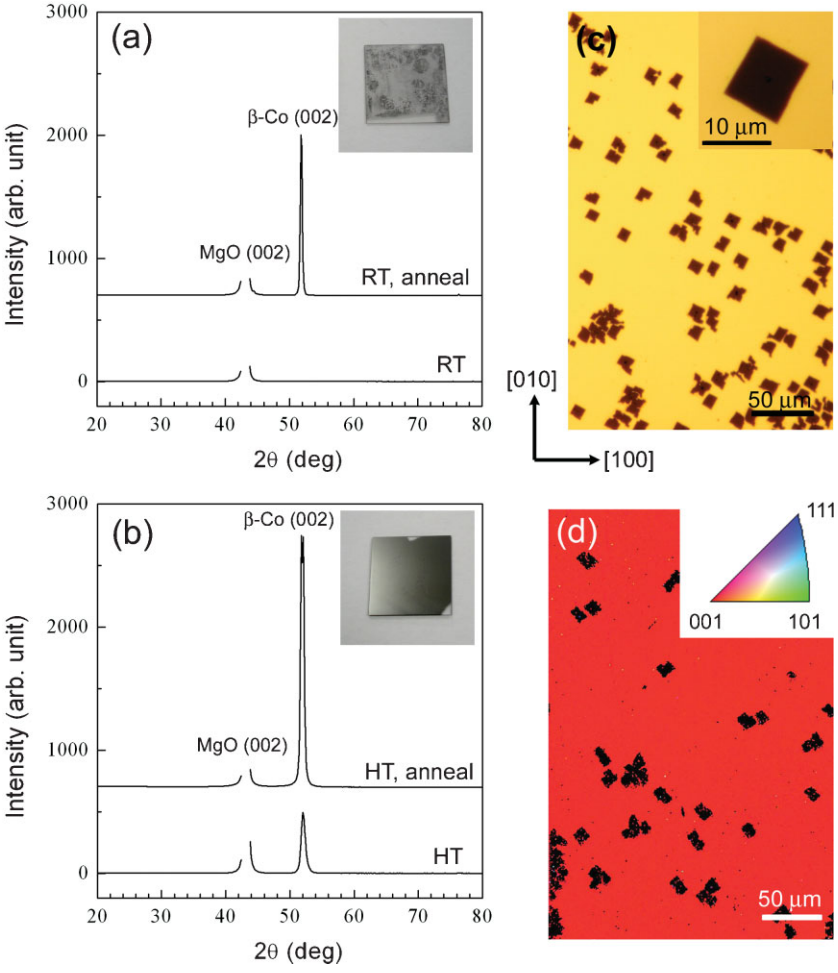

Figure 2. XRD profiles of as-prepared and annealed Co films deposited on MgO(001). The Co films were sputtered at a) room temperature and b) 300 °C. The inset shows a photograph of the substrate after annealing at 900 °C in vacuum. The substrate size is about 10 mm × 10 mm. c) Optical microscopy image and d) EBSD data of the annealed Co/MgO(001) substrate shown in the inset of (b).

2.2. Synthesis of Graphene Films on MgO(001)

For the synthesis of graphene, PS was spin-coated on the epitaxial Co metal sputtered on MgO(001) at high temperature, followed by annealing in high vacuum at 900 °C. As seen in Figure 3a–c, a number of rectangular pits were also observed after annealing in the presence of PS. The density of the rectangular pits was around 500–3000 pits mm^{-2}. The AFM image at the bottom of the pit shows a wrinkle surface (Figure 3d), suggesting a film-like structure. Raman mapping images are displayed in Figure 3e and f. Interestingly, both the G-band (1583 cm^{-1}) and 2D-band (≈2700 cm^{-1}) were mainly observed inside the rectangular pits, suggesting the preferential formation of graphene films. Outside of the rectangular pits, either a very weak and discontinuous Raman signal or no signal was detected. The Raman spectra measured at three different points are shown in Figure 3g. It is reported that the relative intensity of G/2D bands represents the number of layers of graphene; the relative intensity of G to 2D bands increases with increasing number of layers.[25,27,28,32] Based on the previous assignment, the films at points B and C are estimated to be 2–5 layers of graphene. However, at point A, a low 2D/G ratio was observed, which suggests partial formation of relatively thick film inside the pit.

In Figure 3h and i, three neighboring pits were mapped. These images also support the preferential formation of graphene films inside pits. The thickness of graphene film differs in each pit but, in a number of rectangular pits, Raman spectra of few-layer graphene were observed (Figure S2). Generally, thinner graphene gave a weaker Raman signal with lower signal-to-noise (S/N) ratio under the same measurement conditions. Figures 3j–l and S3 show cross-sectional transmission electron microscopy (TEM) images measured for the sample cut from a rectangular pit using a focused ion beam (FIB). These images prove that the formation of graphene layers inside the pit. The thickness depends on the pit and we obtained mainly 2–5 layers but, at some areas, single-layer graphene was observed, as shown in Figure 3k. It is interesting to note that the Co metal was not observed at the interface between graphene and MgO in many pits, which will be discussed later. The formation of the pit structure has already been demonstrated[33] but this is the first time that graphene has been shown to preferentially form inside the pits.

Since Raman spectra of graphene films grown by the CVD method have not been well characterized on metal catalyst films or metal oxide substrates, we transferred as-grown graphene films for more reliable evaluation.[32,34] Dissolving Co metal catalyst in a dilute HCl solution gave floating graphene films on the surface of the HCl solution. These floating films were caught by a SiO_2/Si substrate by immersing the substrate into the solution, although the films were too small to observe by eye. An AFM image of a transferred film is shown in Figure 4. Note that the rectangular shape was maintained even after the transfer process. This signifies the formation of a continuous graphene film inside a rectangular pit. The height of the transferred film was determined to be ≈1.3 nm from the AFM imaging, proving the transfer of few-layer graphene. We observed that the graphene transferred onto the SiO_2/Si substrate gives a stronger Raman signal than the as-grown graphene on the Co pits, as seen in Figure 4c. This is consistent with the previous report on the substrate dependence of Raman intensity.[34] The D-band, which is associated with defects in graphene network, became stronger after the transfer, indicating the introduction of damage to the graphene during the transfer process. This transfer method frequently gave folded graphene films, as shown in the Supporting Information (Figure S4), except for

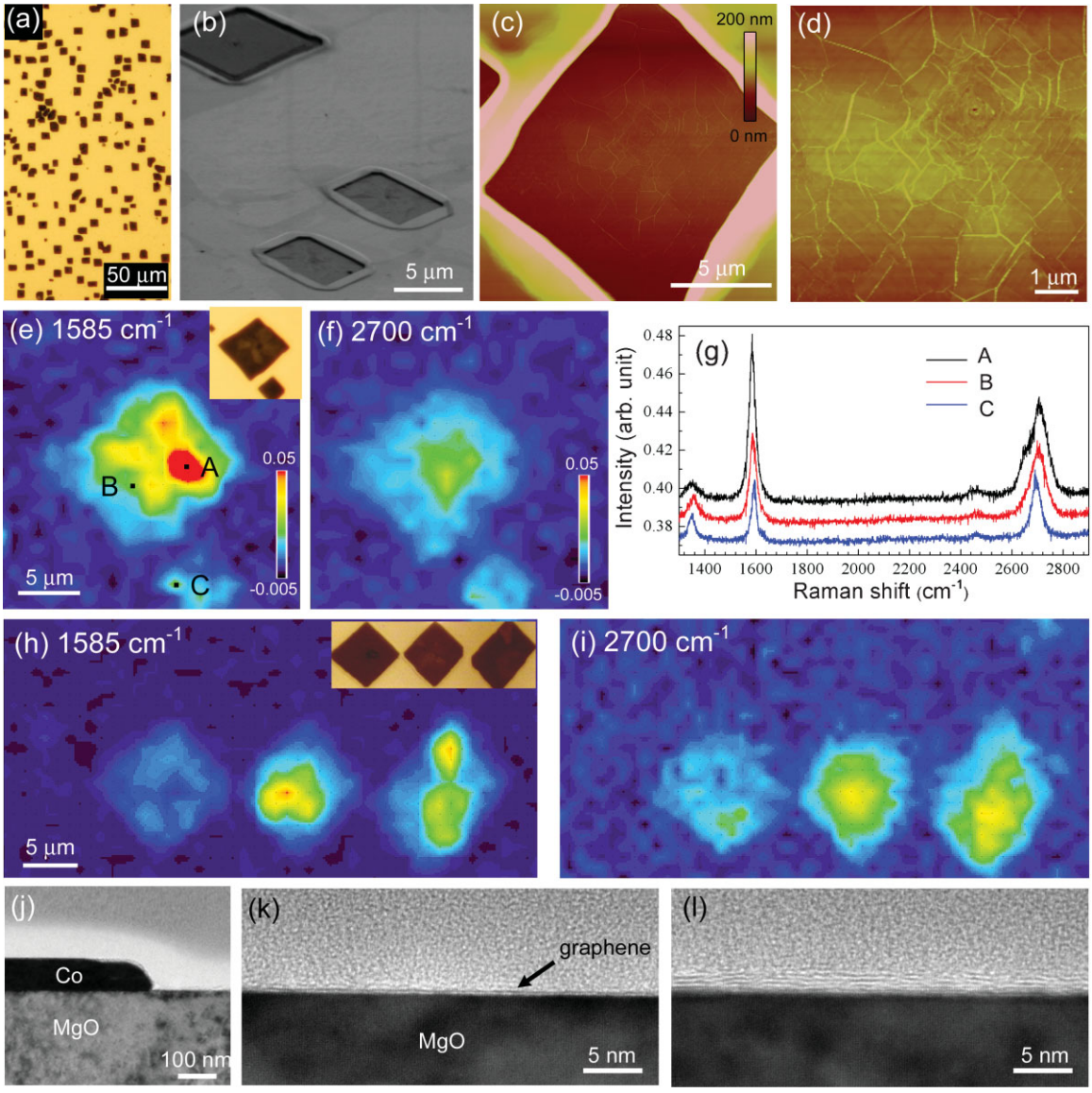

Figure 3. a) Optical microscopy, b) SEM, and c,d) AFM images of the rectangular pits formed after thermal treatment of PS on the epitaxial Co/MgO(001) surface. Spatial Raman intensity of e) the G and f) 2D bands of the rectangular pits. Inset of (e) shows the corresponding optical microscopy image. The excitation wavelength is 514.5 nm. g) Raman spectra measured at the three different points denoted in the mapping image. h,i) Raman mapping images of three neighboring rectangular graphene films shown in (e). j) Cross-sectional TEM image near the pit edge and TEM images of k) single-layer and l) 4–5-layer graphene films formed inside a pit.

relatively thick graphene films, which maintained their original shape. Moreover, the yield of the transfer was very low.

Therefore, for more efficient transfer, we covered the substrate surface with a PMMA film and mechanically stabilized this PMMA film using thermal tape.[35] After dissolving the Co metal catalyst in a HCl solution, the thermal tape/PMMA/graphene film was transferred onto a SiO_2(300 nm)/Si substrate. Finally, the thermal tape and PMMA were removed by baking and dissolving in acetone, respectively. The optical microscopy image of the transferred films is shown in Figure 5a and b. Due to the protective PMMA layer, most of the rectangular graphene maintained its original shape after the transfer process. In addition, the density of the graphene films was nearly same as the original density formed on the Co surface, proving almost 100% transfer yield.

For statistical analysis of the number of graphene layers, the relative G/2D intensity of the Raman spectra were measured for 50 rectangular graphene films transferred using PMMA (Figure 5c). The G/2D intensity varied from 0.8 to 1.5, indicating the predominant formation of 2–5 layers of graphene.[32,36] The full width at half maximum (FWHM) of the 2D-band is plotted in Figure 5d. The 2D FWHM distributes within 42–62 cm^{-1}, which also suggests the formation of 2–5 layers. We also studied the contrast of the optical microscopy image of the transferred graphene films by comparing with that of exfoliated graphene prepared from HOPG (Figure S5).

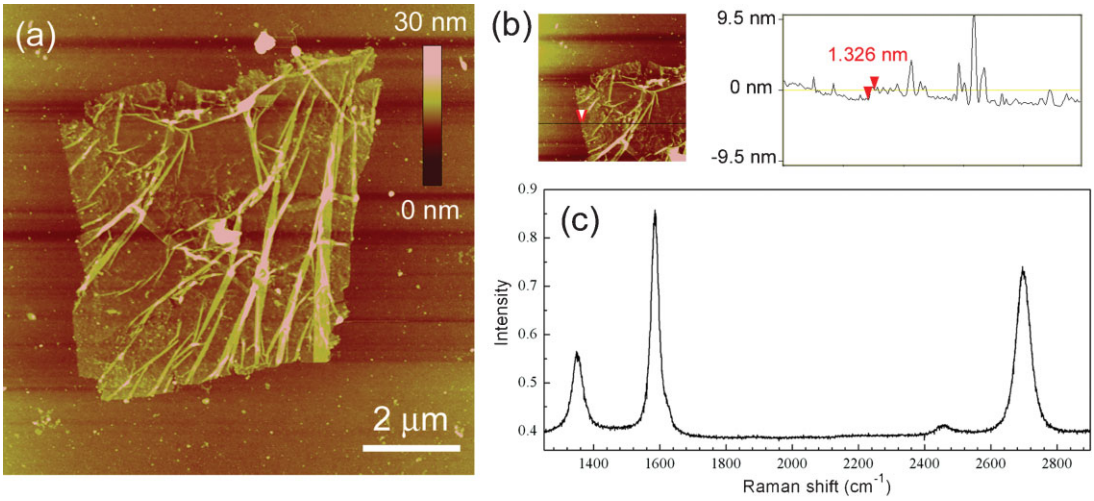

Figure 4. A transferred graphene film deposited on a SiO_2/Si substrate: a) AFM image, b) height profile, and c) Raman spectrum.

Generally, the optical microscopy images show the contrast of few-layer graphene, which is consistent with the Raman data (Figure 5c and d).

2.3. Synthesis of Graphene Films on MgO(111) Substrates and/or Ni Catalysts

We also investigated the graphene growth on the Co film epitaxially deposited on a MgO(111) substrate. Interestingly, triangular pits predominantly appeared on the Co metal surface and consequently, triangularly shaped graphene films were preferentially formed inside these pits. An optical microscopy image of the pits and the Raman mapping images are shown in Figure 6. The orientations of all the pits were the same, which proves the strong epitaxial relationship between the Co film and the MgO substrate. In the case of MgO(111), the formation of triangular pits occurred inhomogeneously; that is, the density varied within the substrate. Locally, a density comparable to the square pits was obtained. Our results show that a macroscopic structure of graphene film can be obtained by using epitaxial metal films without employing any lithographic technique. Raman spectra of edges of rectangular or triangular graphene films are interesting and further study is necessary.

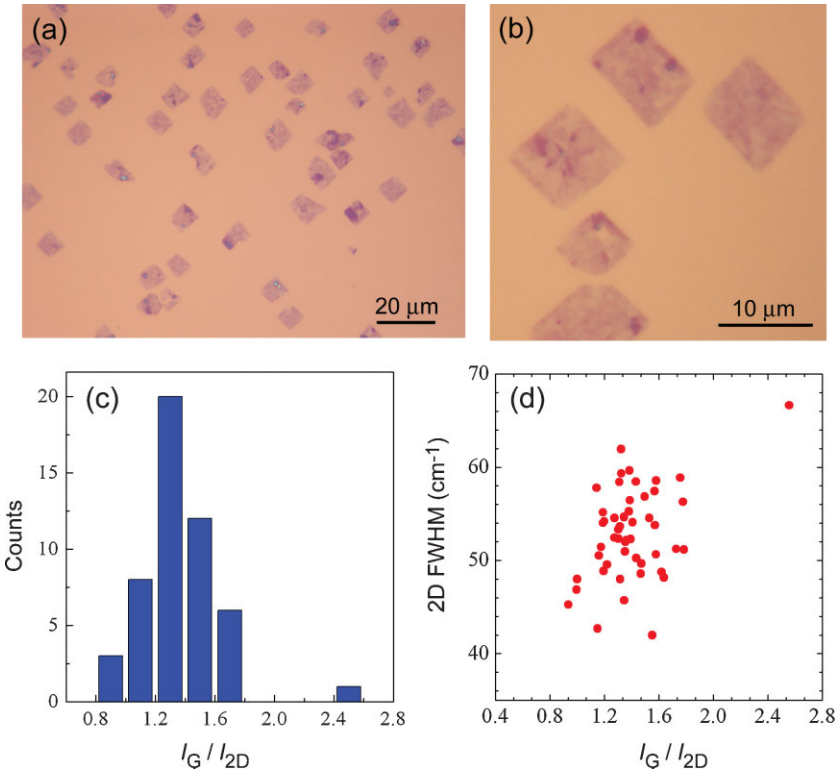

Figure 5. a,b) Optical microscopy images of the rectangular graphene films on a SiO_2/Si substrate. The graphene films were transferred with the aid of a PMMA protective layer. c) Histogram of the relative G/2D intensity measured by Raman spectroscopy for 50 graphene films. d) FWHM of the 2D peak plotted against the relative G/2D ratio.

Epitaxial Ni metal films were studied as a catalyst and we confirmed that rectangular and triangular graphene films were also grown on Ni/MgO(001) and Ni/MgO(111), respectively (see Figure S6). This can be understood by the similar lattice structure of β-Co (lattice constant: 0.354 nm) and Ni (Ni has only a fcc structure: 0.352 nm). Clear differences in the quality of graphene were not observed when compared with Co metal catalysts. This result suggests that our epitaxial metal approach can be applied to other metal catalysts, including Cu.[28]

2.4. Formation Mechanism of Patterned Graphene Films

Here, we discuss the formation mechanism of graphene inside the rectangular/triangular pits on the epitaxial metal film. A proposed growth mechanism is illustrated in Figure 7. The PS film decomposes at elevated temperature and most of the

NANO MICRO small

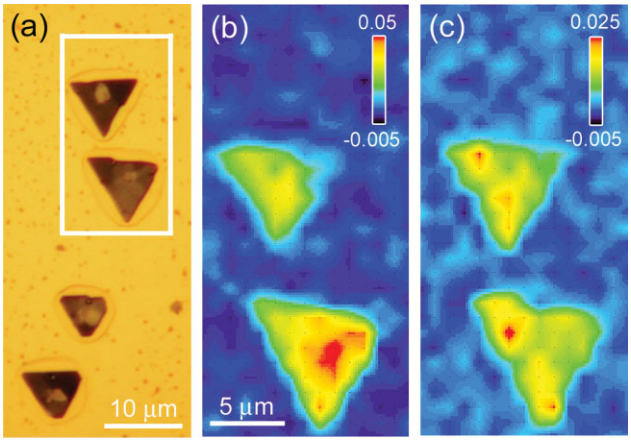

Figure 6. a) Optical microscopy image of triangular pits formed by heating PS/Co/MgO(111) in vacuum. The Raman mapping images of b) the G band and c) the 2D band. The measured area is marked in (a).

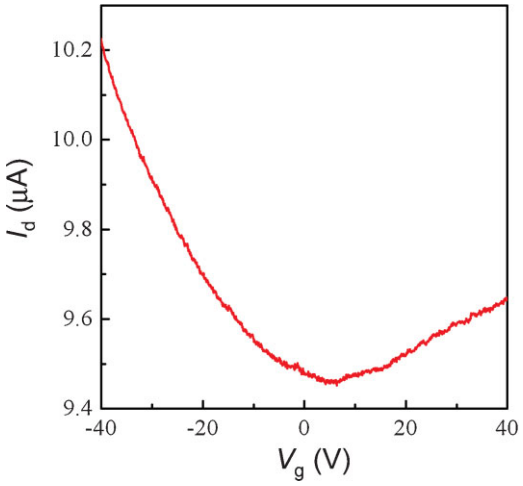

Figure 8. Transfer characteristics of a rectangular graphene film transferred onto a SiO_2/Si substrate. ($V_d = 0.1$ V, channel length and width are 3 mm and 6.5 mm, respectively)

decomposed fragments are expected to be desorbed from the metal surface due to the vacuum conditions. However, some of the decomposed carbon atoms dissolve into the metal. Because the dissolved carbon atoms are regarded as an impurity in the metal, these carbon atoms are discharged from the metal catalyst simultaneously with the formation of the pit structure. We tried to synthesize graphene films by thermally decomposing PS on the preannealed substrate, which has many pits, but no graphene or discontinuous graphene films were observed in the pits. Therefore, we conclude that the pit formation and the graphene growth occur simultaneously. Another possible scenario is the partial penetration of the Co metal into the MgO substrate during the annealing process, similar to the reported thermal diffusion of Fe into MgO matrix for the Fe/MgO-supported catalyst that was used for single-walled carbon nanotube growth.[37] However, since a cross-sectional TEM image (Figure 3j) showed a clear interface between Co and MgO, it is unlikely that the Co metals with 50-nm thickness are dissolved into the MgO substrate.

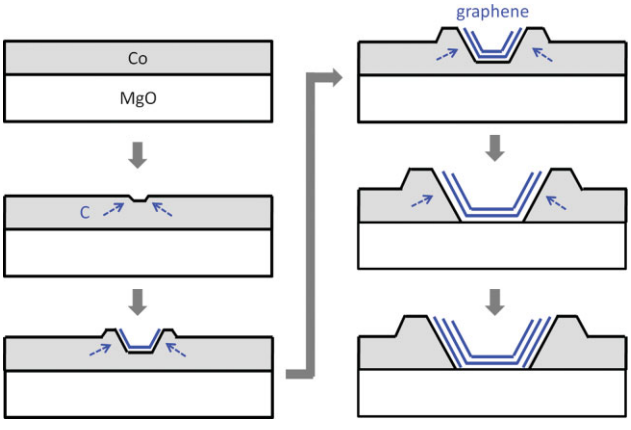

Figure 7. Proposed growth mechanism of few-layer graphene films inside a pit. At the annealing temperature, the pit structure develops together with carbon diffusion, resulting in the formation of graphene inside the pit.

Our proposed mechanism (Figure 7) provides a new means to grow graphene films directly on the insulating substrate, which is important for device fabrication. It is considered that the graphene formation in pits is different to the standard CVD growth, in which carbon precipitation occurs from the planar metal film during the cooling process.[24] The dynamic and synergetic process of carbon precipitation and metal reconstruction observed in the present study would give a new insight into the growth mechanism of graphene. We tried thermal CVD with methane feedstock under atmospheric pressure but it gave a rough surface and inhomogeneous graphene films with no unique regular structures (Figure S7). Thus, our catalytic polymer decomposition offers a new and unique method to synthesize graphene.

2.5. Transport Property

Finally, field-effect transistors (FETs) were fabricated using transferred rectangular graphene films, as depicted in Figure 8. Because of the unique graphene structure, we did not need to use O_2 plasma to etch out a workable area for FET fabrication. Most of the devices showed a weak modulation of the drain current in the range of –40 to 40 V, reflecting a semimetallic or zero-gap-semiconductor electronic structure. The devices showed clear Dirac points, mainly at $V_g \approx 0$–15 V, which is the typical signature of graphene. The n-type conduction was slightly suppressed in our transferred graphene, which can be due to the doping induced by the adsorption of O_2 and/or H_2O.[38] The suppression of n-type conduction was reported by Arco et al. for CVD-grown graphene.[26] Our method provides high-density micrometer-scale graphene films with a specific microstructure and few-layer thickness, so it can be useful for double-gated devices for the control of electronic structure.[6]

3. Conclusions

In this work, we propose, for the first time, the use of epitaxial metal films deposited on a single-crystal substrate as the sacrificing layer for graphene growth. On MgO(001) and

(111) substrates, unique rectangularly and triangularly shaped few-layer graphene films, respectively, were preferentially produced inside the pits. This demonstrates a method to grow specific graphene structures in a self-organized manner. The rectangular/triangular shape does not require any lithographic or etching processes, which are commonly used for large-area graphene synthesis. The preferential formation of graphene films inside these pits suggests the precipitation of carbon atoms at defects/grain boundaries of the epitaxial metal film after diffusion inside the film. Thermal decomposition of the polymer precursor offered a simple route to graphene growth while maintaining the crystallinity of the metal catalyst film. We found that the formation of pits occurred simultaneously with graphene precipitation, which is important for further understanding of the graphene precipitation mechanism. The graphene was successfully transferred onto a Si substrate by using a PMMA film without deforming the original shape. A FET was demonstrated using the transferred graphene film.

4. Experimental Section

Preparation of epitaxial metal films: Co or Ni metal films were deposited on either MgO (001) or (111) substrates by RF magnetron sputtering (Shibaura Mechatoronics Corp., CFS-4ES). During sputtering, the MgO substrate was heated at 300 °C with a power of 200 W under an Ar atmosphere (0.6 Pa). For comparison, sputtering was also performed at RT. The thickness of the sputtered Co (or Ni) film was fixed to be ≈50 nm. The film thickness was calibrated by sputtering onto a substrate patterned with photoresist; after lift off, the film thickness of the metal film was determined by AFM.

Synthesis of graphene films: PS ($M_w = 280\,000$, Aldrich) was first dissolved in THF (0.07 wt%). The solution was spin coated onto the Co/MgO or Ni/MgO substrate with 300–1000-nm thickness. After spin coating, the substrate was annealed in vacuum (≈10^{-4} Pa) at 900 °C for 10–30 min using an infrared furnace (ULVAC Corp., MILA-3000). The heating and cooling rates were 200 °C min^{-1} and ≈300 °C min^{-1}, respectively.

Transfer of graphene films: After thermal annealing, the surface of the Co/MgO substrate was covered with PMMA ($M_w = 1\,000\,000$, Aldrich) by spin coating. Thermal tape (Revalpha, Nitto-Denko) was attached onto the PMMA film. Next, the metal catalyst film was dissolved by dipping into HCl solution (3%) to release the graphene protected with thermal tape and PMMA. After washing with deionized (DI) water, the thermal tape/PMMA/graphene was placed on a SiO_2 (300 nm)/Si substrate. The thermal tape was removed by baking at 120 °C and the PMMA film was dissolved by acetone. We also transferred the graphene films by simply removing the metal catalyst film by the HCl solution without thermal tape/PMMA protective layers. In this case, the floating graphene films were transferred by immersing the SiO_2/Si substrate into the HCl solution followed by washing in DI water. Without the protective layers, most of graphene films were folded during the transfer, as shown in Figure S4.

Characterization of graphene and metal catalysts: Raman spectra and mapping images were measured with a JASCO NRS-2100 using an excitation wavelength of 514.5 nm at ≈1-μm spot size. TEM images were measured with a HITACHI H-9500 at a 300 keV acceleration voltage for the sample sliced with a FIB (HITACHI NB5000). AFM images were measured with a Veeco Nanoscope IIIa. The crystallinity of an epitaxial Co film was measured by XRD at the Kyushu Synchrotron Light Research Center (beam line BL-15) and by a scanning electron microscopy (SEM) system equipped with a EBSD (HITACHI S-3000H, TSL Solutions OIM).

Fabrication and measurement of FETs: Patterns of Au electrodes were deposited on the transferred graphene films after lift off. The back-gated FET measurement was carried out with an semiconductor analyzer (Agilent, B1500A) using a probe station at RT. The measurements were carried in vacuum (≈5×10^{-4} Pa).

Acknowledgements

This work was supported by the PRESTO of the Japan Science and Technology Agency (JST) and a Grant-in-Aid for Scientific Research from MEXT, Japan. XRD and TEM measurements were performed at Kyushu Synchrotron Light Research Center and Fukuryo Semiconductor Engineering, respectively.

[1] A. K. Geim, K. S. Novoselov, *Nat. Mater.* **2007**, *6*, 183.
[2] Y. Zhang, Y. W. Tan, H. L. Stormer, P. Kim, *Nature* **2005**, *438*, 201.
[3] J. S. Bunch, Y. Yaish, M. Brink, K. Bolotin, P. L. McEuen, *Nano Lett.* **2005**, *5*, 287.
[4] T. Ohta, A. Bostwick, T. Seyller, K. Horn, E. Rotenberg, *Science* **2006**, *313*, 951.
[5] K. S. Novoselov, Z. Jiang, Y. Zhang, S. V. Morozov, H. L. Stormer, U. Zeitler, J. C. Maan, G. S. Boebinger, P. Kim, A. K. Geim, *Science* **2007**, *315*, 1379.
[6] J. B. Oostinga, H. B. Heersche, X. Liu, A. F. Morpurgo, L. M. K. Vandersypen, *Nat. Mater.* **2008**, *7*, 151.
[7] K. I. Bolotin, K. J. Sikes, Z. Jiang, M. Klima, G. Fudenbeg, J. Hone, P. Kim, H. L. Stormer, *Solid State Commun.* **2008**, *146*, 351.
[8] J. R. Williams, L. DiCarlo, C. M. Marcus, *Science* **2007**, *317*, 638.
[9] S. Gilje, S. Han, M. Wang, K. L. Wang, R. B. Kaner, *Nano Lett.* **2007**, *7*, 3394.
[10] J. T. Robinson, M. Zalalutdinov, J. W. Baldwin, E. S. Snow, Z. Wei, P. Sheehan, B. H. Houston, *Nano Lett.* **2008**, *8*, 3441.
[11] F. Schedin, A. K. Geim, S. V. Morozov, E. W. Hill, P. Blake, M. I. Katsnelson, K. S. Novoselov, *Nat. Mater.* **2007**, *6*, 652.
[12] Y. Ohno, K. Maehashi, Y. Yamashiro, K. Matsumoto, *Nano Lett.* **2009**, *9*, 3318.
[13] C. Berger, Z. Song, X. Li, X. Wu, N. Brown, C. Naud, D. Mayou, T. Li, J. Hass, A. N. Marchenkov, E. H. Conrad, P. N. First, W. A. de Heer, *Science* **2006**, *312*, 1191.
[14] G. M. Rutter, J. N. Crain, N. P. Guisinger, T. Li, P. N. First, J. A. Stroscio, *Science* **2007**, *317*, 219.
[15] H. Hibino, H. Kageshima, F. Maeda, M. Nagase, Y. Kobayashi, H. Yamaguchi, *Phys. Rev. B* **2008**, *77*, 75413.
[16] K. V. Emtsev, A. Bostwick, K. Horn, J. Jobst, G. Kellogg, L. Ley, J. L. McChesney, T. Ohta, S. A. Reshanov, J. Röhrl, E. Rotengerg, A. K. Schmid, D. Waldmann, H. B. Weber, T. Seyller, *Nat. Mater.* **2009**, *8*, 203.

[17] W. Norimatsu, M. Kusunoki, *Chem. Phys. Lett.* **2009**, *468*, 52.
[18] Y. Gamo, A. Nagashima, M. Wakabayashi, M. Terai, C. Oshima, *Surf. Sci.* **1997**, *374*, 61.
[19] D. Usachov, A. M. Dobrotvorskii, A. Varykhalov, O. Rader, W. Gudat, A. M. Shikin, V. K. Adamchuk, *Phys. Rev. B* **2008**, *78*, 85403.
[20] S. Marchini, S. Günther, J. Wintterlin, *Phys. Rev. B* **2007**, *76*, 75429.
[21] P. W. Sutter, J. I. Flege, E. A. Sutter, *Nat. Mater.* **2008**, *7*, 406.
[22] Y. Pan, H. Zhang, D. Shi, J. Sun, S. Du, F. Liu, H. Gao, *Adv. Mater.* **2009**, *21*, 2777.
[23] A. T. N'Diaye, S. Bleikamp, P. J. Feibelman, T. Michely, *Phys. Rev. Lett.* **2006**, *97*, 215501.
[24] Q. Yu, J. Lian, S. Siriponglert, H. Li, Y. P. Chen, S. S. Pei, *Appl. Phys. Lett.* **2008**, *93*, 113103.
[25] A. Reina, X. Jia, J. Ho, D. Nezich, H. Son, V. Bulovic, M. S. Dresselhaus, J. Kong, *Nano Lett.* **2009**, *9*, 30.
[26] L. G. D. Arco, Y. Zhang, A. Kumar, C. Zhou, *IEEE Trans. Nanotechnol.* **2009**, *8*, 135.
[27] K. S. Kim, Y. Zhao, H. Jang, S. H. Lee, J. M. Kim, K. S. Kim, J. H. Ahn, P. Kim, J. Y. Choi, B. H. Hong, *Nature* **2009**, *457*, 706.
[28] X. Li, W. Cai, J. An, S. Kim, J. Nah, D. Yang, R. Piner, A. Velamakanni, I. Jung, E. Tutuc, S. K. Banerjee, L. Colombo, R. S. Ruoff, *Science* **2009**, *324*, 1312.
[29] H. Bialas, E. Knoll, *Vacuum* **1994**, *45*, 959.
[30] P. Sandström, E. B. Svedberg, J. Birch, J. E. Sundgren, *Surf. Sci.* **1999**, *437*, L767.
[31] R. A. Lukaszew, Z. Zhang, V. Stoica, R. Clarke, *Appl. Surf. Sci.* **2003**, *219*, 74.
[32] A. C. Ferrari, J. C. Meyer, V. Scardaci, C. Casiraghi, M. Lazzeri, F. Mauri, S. Piscanec, D. Jiang, K. S. Novoselov, S. Roth, A. K. Geim, *Phys. Rev. Lett.* **2006**, *97*, 187401.
[33] H. T. Shi, D. Lederman, *Phys. Rev. B* **1998**, *58*, R1778.
[34] Y. Y. Wang, Z. H. Ni, T. Yu, Z. X. Shen, H. M. Wang, Y. H. Wu, W. Chen, A. T. S. Wee, *J. Phys. Chem. C* **2008**, *112*, 10637.
[35] H. Tabata, M. Shimizu, K. Ishibashi, *Appl. Phys. Lett.* **2009**, *95*, 113107.
[36] D. S. Lee, C. Riedl, B. Krauss, K. Klitzing, U. Starke, J. H. Smet, *Nano Lett.* **2008**, *8*, 4320.
[37] H. Ago, K. Nakamura, N. Uehara, M. Tsuji, *J. Phys. Chem. B* **2004**, *108*, 18908.
[38] M. Lafkioti, B. Krauss, T. Lohmann, U. Zschieschang, H. Klauk, K. v. Klitzing, J. H. Smet, *Nano Lett.* **2010**, *10*, 1149.

Received: December 29, 2009
Revised: March 29, 2010
Published online: May 19, 2010

